ANNALS of Clinical and Translational Neurology
Open Access
AMERICAN NEUROLOGICAL ASSOCIATION

RESEARCH ARTICLE

# Cardiac sympathetic innervation and vesicular storage in pure autonomic failure

David S. Goldstein[1], Risa Isonaka[1], Courtney Holmes[1], Yu-Shin Ding[2] & Yehonatan Sharabi[3]

[1]Autonomic Medicine Section, Clinical Neurosciences Program, Division of Intramural Research, National Institute of Neurological Disorders and Stroke, National Institutes of Health, Bethesda, MD
[2]Department of Radiology, New York University Langone Medical Center, New York, NY
[3]Department of Internal Medicine, Chaim Sheba Medical Center, Tel Aviv University Sackler Faculty of Medicine, Tel Aviv, Israel

**Correspondence**
David S. Goldstein, Autonomic Medicine Section, CNP/DIR/NINDS/NIH, 9000 Rockville Pike MSC-1620, Building 10 Room 8N260, Bethesda, MD 20892-1620 USA. Tel: 301-496-2103; Fax: 301-402-0180; E-mail: goldsteind@ninds.nih.gov

**Funding Information**
This research was supported by the Intramural Research Program of the NIH, National Institute of Neurological Disorders and Stroke.

Received: 16 July 2020; Revised: 7 August 2020; Accepted: 17 August 2020

***Annals of Clinical and Translational Neurology*** **2020; 7(10): 1908–1918**

doi: 10.1002/acn3.51184

## Abstract

**Objective**: Pure autonomic failure (PAF) is a rare disease characterized by neurogenic orthostatic hypotension (nOH), absence of signs of central neurodegeneration, and profound deficiency of the sympathetic neurotransmitter norepinephrine. Reports have disagreed about mechanisms of the noradrenergic lesion. Neuropathological studies have highlighted denervation, while functional studies have emphasized deficient vesicular sequestration of cytoplasmic catecholamines in extant neurons. We examined both aspects by a combined positron emission tomographic (PET) neuroimaging approach using $^{11}$C-methylreboxetine ($^{11}$C-MRB), a selective ligand for the cell membrane norepinephrine transporter, to quantify interventricular septal myocardial noradrenergic innervation and using $^{18}$F-dopamine ($^{18}$F-DA) to assess intraneuronal vesicular storage in the same subjects. **Methods**: Seven comprehensively tested PAF patients and 11 controls underwent $^{11}$C-MRB PET scanning for 45 minutes (dynamic 5X1', 3X5', 1X10', static 15 minutes) and $^{18}$F-DA scanning for 30 minutes (same dynamic imaging sequence) after 3-minute infusions of the tracers on separate days. **Results**: In the PAF group septal $^{11}$C-MRB-derived radioactivity in the static frame was decreased by 26.7% from control ($p = 0.012$). After adjustment for nonspecific binding of $^{11}$C-MRB, the PAF group had a 41.1% mean decrease in myocardial $^{11}$C-MRB-derived radioactivity ($p = 0.015$). The PAF patients had five times faster postinfusion loss of $^{18}$F-DA-derived radioactivity ($70 \pm 3\%$ vs. $14 \pm 8\%$ by 30 minutes, $p < 0.0001$). At all time points after infusion of $^{18}$F-DA and $^{11}$C-MRB mean $^{18}$F/$^{11}$C ratios in septal myocardium were lower in the PAF than control group. **Interpretation**: PAF entails moderately decreased cardiac sympathetic innervation and a substantial vesicular storage defect in residual nerves.

## Introduction

Pure autonomic failure (PAF), formerly called idiopathic orthostatic hypotension, is a rare disease in which neurogenic orthostatic hypotension (nOH) dominates the clinical picture without clinical signs of central neurodegeneration. The disease can progress to Parkinson disease or dementia with Lewy bodies or can continue for many years manifesting mainly with disabling nOH.[1]

PAF is characterized by profound myocardial norepinephrine (NE) deficiency.[2] Reports have disagreed about mechanisms of the cardiac noradrenergic lesion. A postmortem study using semiquantitative immunohistochemical methodology noted severely decreased immunoreactive tyrosine hydroxylase (TH), a marker of catecholamine-synthesizing neurons, in epicardial nerves of one PAF patient.[3] On the other hand, in vivo studies based on $^{18}$F-dopamine ($^{18}$F-DA) positron emission tomographic (PET) scanning and arterial plasma levels of catechols have noted evidence for a vesicular storage defect, with a shift from vesicular sequestration to enzymatic deamination of cytoplasmic $^{18}$F-DA in cardiac sympathetic nerves.[4] A recent study reported that PAF patients had normal protein levels of the cell membrane

NE transporter (NET) in dorsal hand vein tissue, associated with decreased levels of the type 2 vesicular monoamine transporter (VMAT),[5] results that led the authors to ask whether impaired intraneuronal vesicular storage, rather than sympathetic denervation, may explain the noradrenergic deficiency attending PAF, at least early in the disease course. The issue of denervation vs. decreased vesicular storage efficiency is important, because dysfunctional but extant ("sick-but-not-dead")[6] neurons might be salvageable by a form of disease modification.[7]

$^{11}$C-methylreboxetine ($^{11}$C-MRB) is a positron-emitting selective NET ligand[8] that is being used increasingly to examine noradrenergic innervation in clinical disease entities.[9,10] In nonhuman primates, after $^{11}$C-MRB injection myocardial radioactivity begins to accumulate virtually immediately, with a subsequent disappearance half-time of about 25 minutes.[11] Pretreatment with desipramine (DMI), a tricyclic antidepressant that decreases NET availability, attenuates cardiac $^{11}$C-MRB uptake,[11] indicating occupation of NET sites by $^{11}$C-MRB.

Since $^{11}$C-MRB does not enter neurons, $^{11}$C-MRB PET scanning alone cannot evaluate intraneuronal vesicular storage. Meanwhile, although $^{18}$F-DA is an established cardiac sympathetic neuroimaging agent, and accelerated loss of $^{18}$F-DA-derived radioactivity by analysis of dynamic PET images can identify decreased vesicular storage,[12] $^{18}$F-DA PET scanning alone cannot separate a vesicular storage defect from such a defect plus concurrent denervation.

Therefore, in this study we conducted PET scanning after administration of both $^{11}$C-MRB and $^{18}$F-DA to PAF and control subjects. We hypothesized that cardiac noradrenergic deficiency in PAF reflects a combination of sympathetic noradrenergic denervation and a vesicular storage defect in residual terminals. We expected that myocardial concentrations of both $^{11}$C-MRB- and $^{18}$F-DA-derived radioactivity would be decreased in PAF compared to control subjects and that the extent of decrease in $^{18}$F-DA-derived radioactivity would be greater than the decrease in $^{11}$C-MRB- derived radioactivity in the PAF patients.

The concept diagrams in Figure 1 depict the rationale for the study. Cardiac sympathetic denervation alone should equivalently decrease myocardial $^{11}$C-MRB- and $^{18}$F-DA-derived radioactivity (equivalently smaller objects and circles in Figure 1B). If there were both sympathetic denervation and a vesicular storage defect in residual nerves, there would be greater loss of $^{18}$F-DA-derived radioactivity than of $^{11}$C-MRB-derived radioactivity (Figure 1C). A combination of denervation with a vesicular storage defect would also decrease peak $^{18}$F-DA-derived radioactivity and accelerate the loss of radioactivity (Figure 1E).

Previous studies have not used $^{11}$C-MRB PET scanning to visualize cardiac sympathetic innervation in humans. To validate $^{11}$C-MRB PET as a means to quantify NET binding sites in humans we administered $^{11}$C-MRB to DMI-pretreated healthy volunteers. We also measured cardiac $^{11}$C-MRB-derived radioactivity in individuals who had undergone cardiac transplantation. The donor heart would be expected to have no sympathetic innervation in the inferior wall and therefore have decreased $^{11}$C-MRB-derived radioactivity. Reinnervation can occur over years at the base of the heart but does not extend to the apical inferior wall.[13] To assess intraneuronal alpha-synuclein deposition, myocardial noradrenergic deficiency, and sympathetic denervation in PAF, postmortem data are included from one of the PAF patients who died about 2 years after undergoing $^{11}$C-MRB scanning.

## Subjects/Materials and Methods

### Subjects

The subjects in this study were evaluated at the National Institutes of Health Clinical Center after having given written informed consent to participate in one or more research protocols approved by the Institutional Review Board of the National Institute of Neurological Disorders and Stroke. The Radiation Safety Committee of the National Institutes of Health approved our use of radioactivity for research purposes.

All the PAF patients (N = 7) had been referred for OH as a manifestation of chronic autonomic failure. PAF was diagnosed by nOH without a known secondary cause and no signs of central neurodegeneration.[14] In addition, all the patients had interventricular septal myocardial $^{18}$F-DA-derived radioactivity less than 6,000 nCi-kg/cc-mCi, as is typical of PAF.[15] This was appropriate to address the issue of denervation vs. a vesicular storage defect as determinants of low $^{18}$F-DA-derived radioactivity.

The PAF patients underwent comprehensive clinical laboratory testing that included analyses of skin biopsies taken from the nape of the neck. The skin biopsy tissues were assayed for colocalization of immunoreactive alpha-synuclein (AS) with TH as described previously[16] to confirm that the patients had intraneuronal AS deposition as expected in a Lewy body disease.

The control subjects (N = 11) were adults who did not have OH, had no evidence of central neurodegeneration, and had unremarkable results of miscellaneous screening laboratory and autonomic function tests. Four controls were healthy volunteers (HVs); the remainder had hypertension but were otherwise healthy.

Two other subjects (61 and 62 year old men) underwent $^{18}$F-DA and $^{11}$C-MRB scanning about 3 years after cardiac transplantation for end-stage ischemic cardiomyopathy.

 

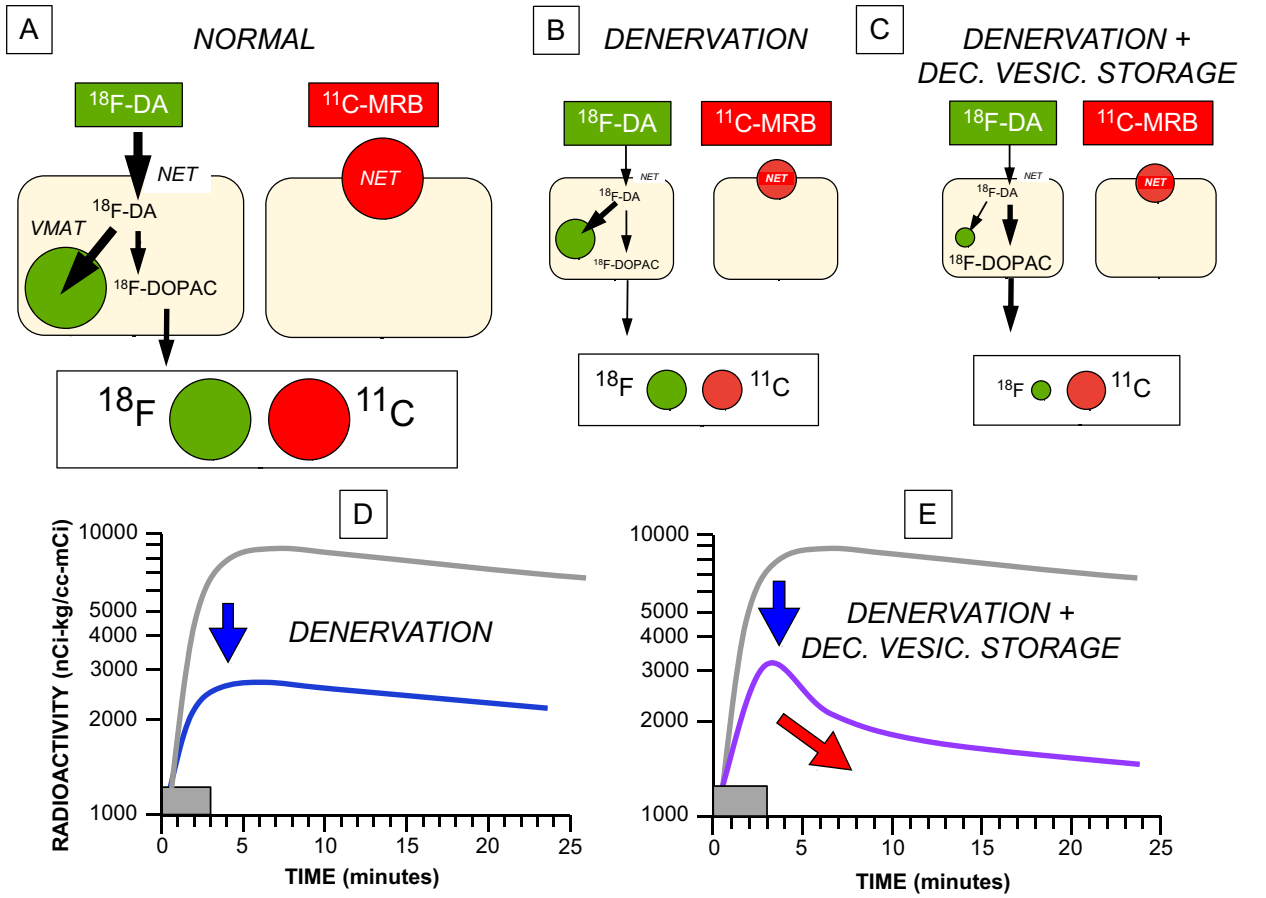


**Figure 1.** Concept diagrams for the effects of cardiac sympathetic denervation with or without decreased vesicular storage on myocardial radioactivity after administration of $^{18}$F-dopamine ($^{18}$F-DA) or $^{11}$C-methylreboxetine ($^{11}$C-MRB). (A) When there is intact innervation *(NORMAL),* $^{18}$F-DA is taken up into sympathetic nerves via the cell membrane norepinephrine transporter (NET). Cytoplasmic $^{18}$F-DA is then mainly taken up into vesicles via the vesicular monoamine transporter (VMAT), with a minor alternative fate oxidative deamination to form $^{18}$F-dihydroxyphenylacetic acid ($^{18}$F-DOPAC), which rapidly exits the neurons. $^{11}$C-MRB binds to the NET but does not enter the neurons. Myocardial $^{11}$C-MRB-derived radioactivity reflects high-affinity NET binding. (B) Denervation *(DENERVATION)* equivalently decreases $^{18}$F-DA- and $^{11}$C-MRB-derived radioactivity (equally small green and red circles). The objects in (B) and (C) are smaller than those in (A), to convey the loss of sympathetic neurons. (C) Combined denervation with decreased vesicular storage *(DENERVATION + DEC. VESIC. STORAGE)* reduces $^{18}$F-DA-derived radioactivity more than $^{11}$C-MRB-derived radioactivity. (D) Effects of denervation on $^{18}$F-DA-derived radioactivity as a function of time. The gray rectangles show the 3-minute period of intravenous infusion of the tracer. Denervation shifts downward the curve relating the log of $^{18}$F-DA-derived radioactivity vs. time (from gray line to blue line), without a change in slope. (E) Combined denervation and decreased vesicular storage decreases peak radioactivity and accelerates the loss of radioactivity (purple line).

## PET scanning

$^{18}$F-DA scanning was done as described previously[17] using a GE Advance™ or Siemens Biograph 128 PET/CT scanner. One mCi of the tracer was administered intravenously via an infusion pump over 3 minutes. Attenuation correction was accomplished by transmission scanning using a rotating pin source for the GE Advance™ scanner and computed tomography for the Siemens scanner. The scanners were calibrated using phantoms as part of routine quality control procedures. Dynamic frames were obtained (5 X 1-minute, 3 X 5-minute, and 1 10-minute duration) over 30 minutes. The delay to scan start was about 30 seconds.

$^{11}$C-MRB scanning was done as for $^{18}$F-DA scanning, with 10 mCi of $^{11}$C-MRB (specific activity about 74 X 104 MBq/μmole at the time of injection) injected intravenously over 3 minutes. The dynamic scanning sequence was followed immediately by a static 15-minute scan, so that the total duration of $^{11}$C-MRB scanning was 45 minutes from the start of tracer administration.

All the PAF patients also underwent thoracic PET scanning after administration of the perfusion imaging agent $^{13}$N-ammonia, to confirm homogeneous perfusion in the

 

left ventricular myocardium and facilitate placement of regions of interest in the $^{18}$F-DA scan images. After rapid IV injection of 5 mCi of $^{13}$N-ammonia a total of 22 dynamically obtained frames were obtained, with a last 5-minute frame having its mid-point about 8 minutes after initiation of tracer injection.

The PAF patients had brain $^{18}$F-DOPA PET scanning, to evaluate striatal dopaminergic innervation. Each PAF patient received 7 mCi of $^{18}$F-DOPA intravenously over 3 minutes, without carbidopa pretreatment. A static 15-minute scan was obtained, with the end of the scanning 120 minutes after initiation of tracer administration. In most patients magnetic resonance imaging was done to aid placement of regions of interest (ROIs).

### DMI

Four healthy volunteers (one man, three women, mean age 50 ± 4 years old, age range 40-55 years old) underwent $^{11}$C-MRB scanning twice, once without and once with DMI pretreatment (125 mg by mouth about 2 hours prior to $^{11}$C-MRB administration).

### Data analysis and statistics

Analyses of the PET images and assays of the catechols in plasma were done by personnel who were blinded as to the diagnostic group until the results had been tabulated.

ROIs in the PET scan images were drawn by hand in the septum and left ventricular. The borders of the ROIs in the walls of the heart were placed to surround areas with the highest uniform radioactivity. ROIs in $^{18}$F-DOPA scans were drawn by hand in the putamina and occipital cortices on both sides of the brain in the static 15-minute scan ending at 120 minutes. Radioactivity concentrations were adjusted for the radioactivity dose per kg body mass and expressed in units of nCi-kg/cc-mCi (numerically equivalent to $10^{-6}$ kg/cc).

Independent-means t-tests were used to compare the PAF and control group in values for interventricular septal myocardial and left ventricular chamber $^{18}$F-DA- and $^{11}$C-MRB-derived radioactivity. Independent-means t-tests were done for septal $^{18}$F/$^{11}$C ratios for each of the dynamic frames after the tracer infusions. To take into account multiple comparisons, Bonferroni's correction was used. For the seven comparisons the p value to define statistical significance was 0.0071.

Dependent-means t-tests were used to compare DMI pretreatment vs. no DMI pretreatment.

Nonspecific binding of $^{11}$C-MRB-derived radioactivity would be expected to interfere with the interpretation of cardiac $^{11}$C-MRB PET data. To adjust for nonspecific binding of $^{11}$C-MRB, chamber radioactivity (equivalent to coronary intraarterial radioactivity) was subtracted from concurrent septal radioactivity at each time point.

Mean values for group data were expressed ± 1 standard error of the mean (SEM).

## Results

### Group characteristics

Table 1 shows individual values for demographic and laboratory values in the PAF group. All the PAF patients had normal septal $^{13}$N-ammonia-derived radioactivity, elevated AS-TH colocalization indices in skin biopsies,[16] and normal PUT/OCC ratios of $^{18}$F-DOPA-derived

**Table 1.** Clinical and laboratory characteristics of PAF patients.

| Patient # | Age | Sex | $^{13}$N-NH$_3$ | $^{18}$F-DA | UPDRS | UPSIT | PUT/OCC | Coloc. |
|---|---|---|---|---|---|---|---|---|
| 1 | 79 | F | 6529 | 3775 | 6 | 20 | 2.79 | 4.74 |
| 2 | 57 | F | 8545 | 3194 | 16 | 15 | 3.01 | 2.06 |
| 3 | 63 | M | 8378 | 3110 | 11 | 19 | 2.89 | 3.7 |
| 4 | 71 | F | 9669 | 4157 | 7 | 30 | 2.73 | 3.07 |
| 5 | 77* | M | 8225 | 4498 | 70 | 13 | 2.13 | 1.60 |
| 6 | 77 | M | 7497 | 3199 | 8 | 23 | 2.71 | 2.36 |
| 7 | 70 | M | 7894 | 3282 | 6 | 26 | 4.05 | 1.61 |
| **Mean** | **71** | **4M, 3F** | **8105** | **3602** | **18** | **23** | **2.6** | **2.63** |
| **Normal** | | | | **>6000**[15] | | | **>2.70**[40] | **<1.50**[16] |

Notes: (*) PAF evolved into dementia with Lewy bodies. Abbreviations: Coloc.=AS-TH colocalization index; $^{18}$F-DA = $^{18}$F-dopamine; F = female; M = male; PUT/OCC = putamen/occipital cortex ratio of $^{18}$F-DOPA-derived radioactivity; $^{13}$N-NH$_3$ = $^{13}$N-ammonia; $^{18}$F-dopamine; $^{11}$C-MRB = $^{11}$C-methylreboxetine; UPDRS = Uniform Parkinson's Disease Rating Scale; UPSIT = University of Pennsylvania Smell Identification Test. Normal values for $^{18}$F-DA-derived radioactivity, PUT/OCC, and Coloc. have superscripts. Listing is in chronological order by date of $^{11}$C-MRB scanning. Tabulated values for $^{13}$N-NH$_3$- and $^{18}$F-DA-derived radioactivity are for the 5-minute dynamic frames beginning 5 minutes after initiation of tracer administration. Bolded text in the row beginning with **Mean** are summary values for the PAF group. Bolded text in the row beginning with **Normal** are normal values, with literature citations.

 

**Table 2.** Mean (± SEM) left ventricular chamber concentrations of $^{18}$F-dopamine ($^{18}$F-DA)- and $^{11}$C-methylreboxetine ($^{11}$C-MRB)-derived radioactivity (in nCi-kg/cc-mCi) as a function of time in controls subjects and patients with pure autonomic failure (PAF).

| Time *minutes* | Control $^{18}$F-DA | PAF $^{18}$F-DA | Control $^{11}$C-MRB | PAF $^{11}$C-MRB |
|---|---|---|---|---|
| 1 | 4898 ± 565 | 4606 ± 352 | 1578 ± 460 | 1184 ± 168 |
| 2 | 6868 ± 521 | 7700 ± 783 | 4957 ± 517 | 5359 ± 338 |
| 3 | 7804 ± 475 | 9034 ± 1286 | 5189 ± 449 | 5691 ± 882 |
| 4 | 5571 ± 656 | 6065 ± 552 | 5172 ± 496 | 5961 ± 1134 |
| 5 | 4003 ± 335 | 4364 ± 349 | 3361 ± 341 | 4356 ± 648 |
| 8 | 3403 ± 252 | 3024 ± 197 | 1825 ± 119 | 2333 ± 365 |
| 13 | 2832 ± 256 | 2381 ± 300 | 1470 ± 101 | 2109 ± 273 |
| 18 | 2077 ± 254 | 2078 ± 226 | 1376 ± 135 | 1980 ± 217 |
| 25 | 1917 ± 206 | 1815 ± 152 | 1247 ± 81 | 1296 ± 133 |
| 38 | | | 1172 ± 111 | 1452 ± 213 |

There was about a 30-s delay from initiation of the 3-minute infusion to the initiation of scannings. Therefore, the listed time for the first dynamic image (1 minute duration, mid-point at 30 seconds) is 1 minute.

radioactivity, except for Patient #5, in whom PAF had evolved into DLB + OH.

## $^{18}$F-DA PET scanning

In both the PAF and control groups infusion of $^{18}$F-DA resulted in rapid accumulation of radioactivity in the left ventricular chamber (Table 2). Beginning immediately upon cessation of tracer administration, chamber $^{18}$F-DA-derived radioactivity decreased in a multi-exponential manner. The PAF and control groups did not differ in chamber $^{18}$F-DA-derived radioactivity at any time during or after tracer administration.

In the control group septal $^{18}$F-DA-derived radioactivity also increased rapidly (Figure 2A,C), so that by the end of tracer administration septal radioactivity already substantially exceeded chamber radioactivity. In the dynamic 5-minute frame beginning 5 minutes after initiation of tracer infusion, the left ventricular myocardium was clearly distinguished from the chamber in all the control subjects (see illustrative images in Figure 3). After the infusion ended, in controls septal $^{18}$F-DA-derived radioactivity usually continued to increase briefly before declining relatively slowly (Figure 2C).

In the PAF group there was evident attenuation of accumulation of septal $^{18}$F-DA-derived radioactivity compared to the control group (Figure 2A,C). In most of the patients septal $^{18}$F-DA-derived radioactivity began to decline immediately after infusion of the tracer (Figure 2C). All the PAF patients had markedly reduced septal $^{18}$F-DA-derived radioactivity in the 5-minute dynamic frame beginning 5 minutes after initiation of tracer administration ($P < 0.0001$; Table 1). As illustrated in Figure 3, by this time in all the PAF patients' myocardial radioactivity could not be resolved from chamber radioactivity. In the last dynamic frame, which ended 30 minutes from the start of tracer administration, $^{18}$F-DA-derived radioactivity averaged 23% of control (1911 ± 72 vs 8286 ± 603 nCi-kg/cc-mCi; $P < 0.0001$). The percent decrease in $^{18}$F-DA-derived radioactivity between 3 and 30 minutes after initiation of tracer administration was greater in the PAF group (70 ± 3%) than in the control group (14 ± 8%, $P < 0.0001$).

## $^{11}$C-MRB PET scanning

All four healthy volunteers had lower septal $^{11}$C-MRB-derived radioactivity after DMI pretreatment than without DMI pretreatment, by a mean of 39% from control (3506 ± 189 vs 5698 ± 647 nCi-kg/cc-mCi, p = 0.017). Both heart transplant recipients had decreased septal $^{18}$F-DA-derived radioactivity (3,633 and 2,783 nCi-kg/cc-mCi; by a mean of 72% from control) and decreased $^{11}$C-MRB-derived radioactivity (3487 and 2762 nCi-kg/cc-mCi; by a mean of 44% of control) at the bottom of the heart.

In the PAF and control groups $^{11}$C-MRB-derived radioactivity in the left ventricular chamber (Table 2) and interventricular septum (Figure 2B,D) increased rapidly during the 3-minute infusion of the tracer. The groups did not differ in the accumulation of or peak values for $^{11}$C-MRB-derived radioactivity in the chamber (Table 2) or septum (Figure 2D).

After the infusion, left ventricular chamber $^{11}$C-MRB-derived radioactivity decreased rapidly in both the PAF and control groups (Table 2). Septal $^{11}$C-MRB-derived radioactivity declined more slowly, with a slightly more rapid fall in the PAF group (Figure 2B), so that by the static image ending 45 minutes after initiation of tracer administration, septal $^{11}$C-MRB-derived radioactivity was 26.7% lower in the PAF group ($P = 0.012$).

Figure 2E shows curves for septal $^{11}$C-MRB-derived radioactivity adjusted for nonspecific binding by

 

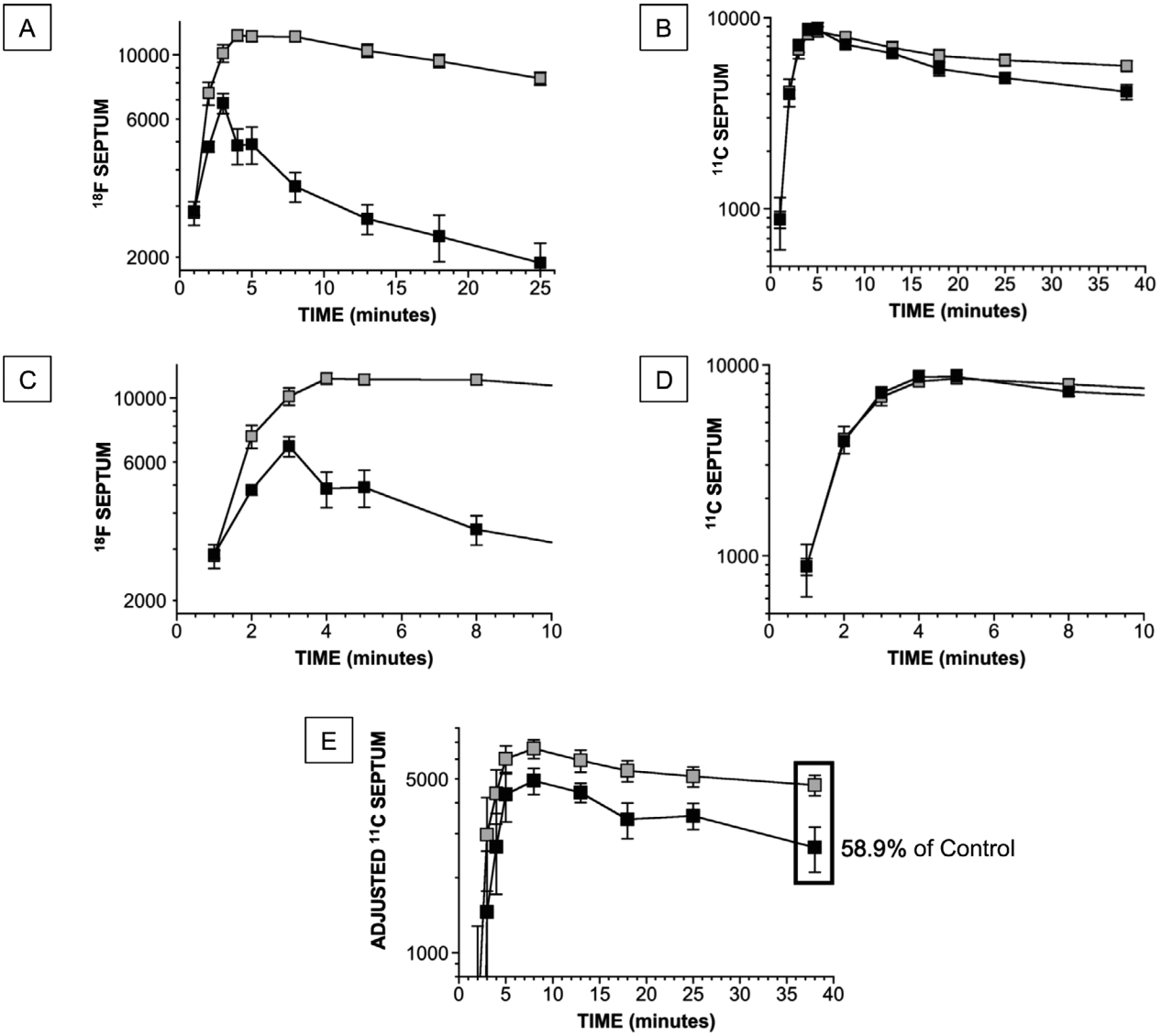


**Figure 2.** Group mean (± SEM) values for cardiac $^{18}$F-DA- and $^{11}$C-MRB-derived radioactivity as a function of time during and after 3-minute intravenous infusion of the tracers. The unit of radioactivity is nCi/cc in regions of interest adjusted for administered radioactivity dose in mCi/kg and therefore is nCi-kg/cc-mCi. Black objects show PAF group and gray objects the control group. A, Septal $^{18}$F-DA-derived radioactivity. B, Septal $^{11}$C-MRB-derived radioactivity. C, D, Same data as for A and B but with expanded time scales. E, Septal $^{11}$C-MRB-derived radioactivity, adjusted by subtracting the concurrent chamber radioactivity. In the static image septal $^{11}$C-MRB-derived radioactivity in the PAF group averaged 58.9% that in the control group (decrease of 41.1% from control).

subtracting the concurrent chamber radioactivity in each subject. In the PAF group, adjusted septal $^{11}$C-MRB-derived radioactivity in the static image was decreased by 41.1% from the control group ($P = 0.015$).

At all time points after infusion of $^{18}$F-DA and $^{11}$C-MRB mean $^{18}$F/$^{11}$C ratios in septal myocardium in the dynamic frames were lower in the PAF than control group (Table 3). When individual values for $^{18}$F/$^{11}$C in the dynamic frames ending 30 minutes after initiation of the 3-minute tracer infusion were expressed as a function of the percent change in $^{18}$F-DA-derived radioactivity in this interval, all the PAF patients had lower values than all the controls for both the $^{18}$F/$^{11}$C ratios and the percent changes in $^{18}$F-DA-derived radioactivity ($P < 0.0001$ by Fisher's exact test; Figure 4).

## Postmortem data

One of the PAF patients (Patient #5) developed DLB and died about 2 years after $^{11}$C-MRB scanning. Postmortem analyses confirmed brainstem Lewy bodies. Sympathetic ganglion tissue had markedly decreased immunoreactive

 

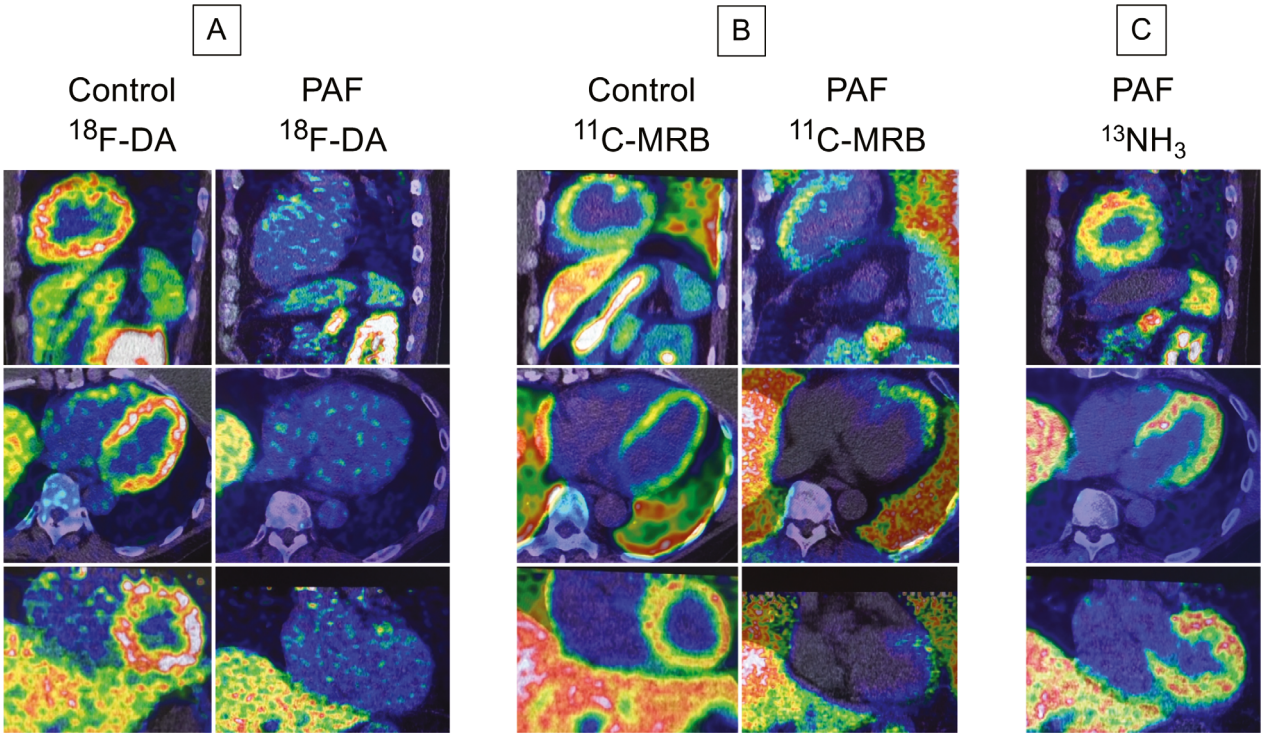


**Figure 3.** Representative $^{18}$F-DA, $^{11}$C-MRB, and $^{13}NH_3$ positron emission/computed tomographic (PET/CT) scans. Shown are cell phone screen shots of fused images displayed on the PET/CT scanner monitor, with spectral color scales in each image adjusted so that the minimum radioactivity is black and maximum white. Top images are sagittal, middle transaxial, and bottom coronal views. Images for $^{18}$F-DA and $^{13}NH_3$ scans were from the dynamic scanning frames from 5-10 minutes after initiation of 3-minute tracer infusion. Images for $^{11}$C-MRB were from a static scan 15-30 minutes after initiation of 3-minute tracer infusion. A, $^{18}$F-DA scans in a control subject and a PAF patient. B, $^{11}$C-MRB scans in the same control subject and PAF patient. C: $^{13}NH_3$ scans in the same PAF patient as in A and B, documenting normal myocardial perfusion. In the PAF patient septal $^{18}$F-DA-derived radioactivity at the bottom of the heart was 28% of control, whereas $^{11}$C-MRB-derived radioactivity was 94% of control.

**Table 3.** Mean (± SEM) ratios of $^{18}$F/$^{11}$C after 3-minute infusions of $^{18}$F-dopamine and $^{11}$C-methylreboxetine in control subjects and patients with pure autonomic failure (PAF)

| Time *min* | Control $^{18}$F/$^{11}$C | PAF $^{18}$F/$^{11}$C | *P* |
|---|---|---|---|
| 0 | 2.77 ± 0.26 | 1.06 ± 0.13 | 0.00065 |
| 1 | 2.13 ± 0.13 | 0.56 ± 0.07 | <0.0001 |
| 2 | 1.74 ± 0.15 | 0.61 ± 0.07 | 0.00015 |
| 5 | 2.00 ± 0.13 | 0.51 ± 0.03 | <0.0001 |
| 10 | 1.88 ± 0.13 | 0.51 ± 0.03 | <0.0001 |
| 15 | 1.82 ± 0.12 | 0.47 ± 0.04 | <0.0001 |
| 22 | 1.84 ± 0.14 | 0.46 ± 0.02 | <0.0001 |

TH and extensive fibrillar deposition of alpha-synuclein. Myocardial NE was decreased by 99% and TH by 97% from control subjects.

## Discussion

In this study $^{11}$C-MRB and $^{18}$F-DA PET scanning was used to evaluate cardiac sympathetic innervation and intraneuronal vesicular storage in PAF. The results indicate that PAF entails a combination of myocardial sympathetic denervation with reduced vesicular sequestration of cytoplasmic catecholamine in residual noradrenergic nerves.

Since this was the first clinical study of cardiac sympathetic neuroimaging by $^{11}$C-MRB scanning, it was necessary to validate the methodology. Decreased $^{11}$C-MRB-derived radioactivity in DMI-treated healthy volunteers and in heart transplant recipients supported the validity of $^{11}$C-MRB scanning to visualize NET binding and therefore cardiac sympathetic innervation. Larger decreases in $^{18}$F- than $^{11}$C-MRB-derived radioactivity in the heart transplant recipients were consistent with newly formed nerves being functionally immature.[18]

Postmortem data in one of the PAF patients confirmed Lewy body pathology, alpha-synuclein deposition in sympathetic ganglion tissue, and extreme cardiac noradrenergic deficiency and sympathetic denervation. These results add to those in several case reports[19-21] and series.[22,23]

The nosology and defining features of PAF remain unsettled.[24] For one thing, how can PAF be defined in

 

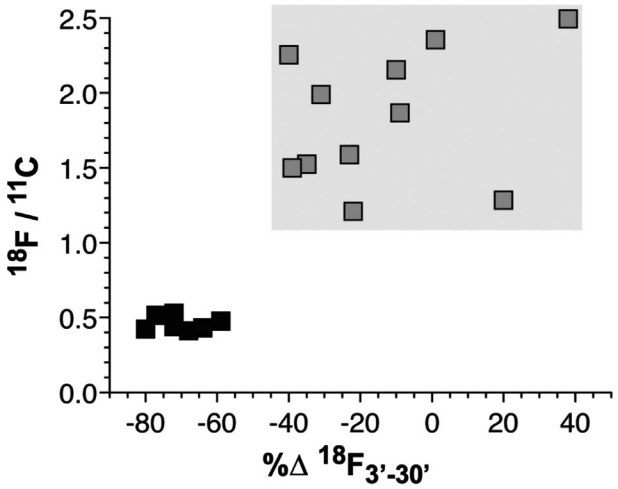


**Figure 4.** Individual values for $^{18}F/^{11}C$ ratios vs. percent changes in $^{18}F$-DA-derived radioactivity between 3 and 30 minutes after initiation of tracer infusion ($\%\Delta^{18}F_{3'-30'}$) in PAF patients (black) and control subjects (gray). (A) The gray rectangle shows the ranges of values in the control group. Note low $^{18}F/^{11}C$ ratios and low values for $\%\Delta^{18}F_{3'-30'}$ values in all the PAF patients compared to all the control subjects.

terms of not involving signs of central neurodegeneration, when PAF patients often have olfactory dysfunction?[25] Another unsettled issue is whether PAF should be considered to be a Lewy body disease.[24] The frequency with which PAF represents a "prodromal" condition is also unclear.[1] These concerns, however, do not invalidate the present data. The PAF patients in this study all had a Lewy body disease, as they all had intraneuronal alpha-synuclein deposition in sympathetic nerves in skin biopsies. We selected these patients, because they all had neuroimaging evidence of cardiac noradrenergic deficiency, and the purpose of the study was to assess denervation and a vesicular storage defect as determinants of that deficiency.

Based on interventricular septal $^{11}C$-MRB-derived radioactivity in the static 15-minute frame ending 45 minutes after initiation of tracer administration, PAF entailed a 26.7% decrease in innervation. This value likely underestimated the actual loss of noradrenergic nerves because of nonspecific binding of $^{11}C$-MRB. Normal accumulation of radioactivity in interventricular septum in the PAF group (Figure 2G) would be explained best if in the human heart there were not only relatively scarce, high-affinity, low-capacity NET binding sites for $^{11}C$-MRB but also relatively abundant low-affinity, high-capacity binding sites. The amount of nonspecific binding would be expected to vary linearly with the concentration of $^{11}C$-MRB in the blood delivered to the myocardium via coronary perfusion, which is equivalent to the concentration in the left ventricular chamber. During infusion of the tracer, essentially all the $^{11}C$-MRB-derived radioactivity in the myocardium would reflect nonspecific binding of $^{11}C$-MRB delivered via the coronary arterial blood. To adjust for nonspecific binding, at each time point in each subject we subtracted the left ventricular chamber radioactivity from the total septal radioactivity. When this was done, by 45 minutes from initiation of tracer administration there was a 41.1% decrease in adjusted septal $^{11}C$-MRB-derived radioactivity in the PAF group compared to the control group.

Few autopsy studies have assessed the status of sympathetic noradrenergic innervation in PAF. Older reports, which referred to the condition as idiopathic orthostatic hypotension, noted decreased catecholamine fluorescence in extracardiac tissues,[26,27] but this methodology cannot separate denervation from decreased ability to store catecholamines in vesicles, because virtually all the catecholamine in sympathetic nerves is in vesicles. The only prior report about cardiac sympathetic innervation in PAF was in a study by Orimo et al., who noted decreased epicardial TH in a single PAF patient without quantifying the extent of decrease.[3] Thus, no postmortem studies are available with which to compare the present estimate of about a 40% decrease in myocardial noradrenergic innervation in vivo in PAF. Semiquantitative analyses of immunoreactive dopamine-beta-hydroxylase (DBH), a marker of sympathetic noradrenergic nerves, in skin biopsies have revealed decreased DBH in sympathetic noradrenergically innervated constituents in PAF,[28,29] but this approach cannot separate denervation from decreased vesicle populations in extant nerves, because DBH is localized to the vesicles.

Between the end of the 3-minute infusion of $^{18}F$-DA and 30 minutes, septal myocardial radioactivity decreased by 70% in the PAF group—about five times the rate of loss observed in the control group. The same PAF patients also had clearly greater loss of myocardial $^{18}F$-DA-derived than of $^{11}C$-MRB-derived radioactivity. The results by the two neuroimaging approaches reinforce each other (Figure 4) in supporting the inference of a substantial vesicular storage defect in cardiac sympathetic nerves in PAF.

In the PAF group septal $^{18}F$-DA-derived radioactivity began to decline immediately after infusion of the tracer. Normally, radioactivity continues to increase for a few minutes,[30] because of ongoing delivery of $^{18}F$-DA via the arterial blood. In essence, early on the vesicles sympathetic nerves act as a sink for $^{18}F$-DA-derived radioactivity. The immediate decline in radioactivity after cessation of the infusion in the PAF group was consistent with decreased ability for radioactivity to accumulate in the neuronal sink, due to a vesicular storage defect.

 

It is important to recognize that low $^{18}$F-DA-derived radioactivity does not imply decreased neuronal uptake of the tracer. For instance, blocking intraneuronal vesicular uptake substantially decreases $^{18}$F-DA-derived radioactivity without any decrease in transport across the cell membrane. This was made clear in previous studies of animals treated with reserpine, which selectively blocks vesicular uptake of cytosolic monoamines.[31,32] Previous clinical studies were not able to distinguish decreased uptake from decreased vesicular storage after normal uptake of $^{18}$F-DA as determinants of low $^{18}$F-DA-derived radioactivity. The multi-tracer imaging approach used here enabled separate assessments of these different processes for the first time.

One might ask why we did not use $^{123}$I-metaiodobenzylguanidine ($^{123}$I-MIBG) as the cardiac sympathetic neuroimaging agent, since $^{123}$I-MIBG is widely available and much more frequently used than $^{18}$F-DA. Single photon emission computed tomographic scanning for measuring $^{123}$I-MIBG-derived radioactivity has insufficient time resolution. What has been referred to as the "uptake" phase of $^{123}$I-MIBG imaging[33-35] takes place over far too long a time frame (in the range of 15-30 minutes) for the $^{123}$I-MIBG-derived radioactivity to reflect neuronal uptake cleanly without a contribution of intraneuronal vesicular uptake.

Positron-emitting analogs of the VMAT2 inhibitor tetrabenazine (e.g., $^{18}$F-dihydrotetrabenazine, $^{11}$C-dihydrotetrabenazine) might have been an alternative to $^{11}$C-MRB, since VMAT2 ligands have been used successfully in several studies to assess intraneuronal vesicular uptake in the brain;[36-38] however, these agents also cannot distinguish a vesicular storage defect from denervation; moreover, there seems to be relatively little cardiac compared to brain uptake of $^{18}$F-dihydrotetrabenazine in humans.[39]

### Perspective

If the present estimate were correct that there is an approximately 40% loss of cardiac sympathetic nerves in PAF, then in order to account for drastic myocardial NE deficiency in PAF the majority of residual nerves would have to be dysfunctional—"sick-but-not-dead." Application of a computational modeling approach recently revealed multiple functional abnormalities in cardiac sympathetic nerves of patients with Lewy body diseases.[6] One such abnormality is decreased efficiency of vesicular sequestration of cytoplasmic catecholamines. Multi-tracer cardiac sympathetic neuroimaging combining $^{11}$C-MRB with $^{18}$F-DA scanning might provide a pathophysiologic biomarker by which to track effects of potential disease-modifying treatments of Lewy body diseases such as PAF.[7] From these results we propose that improving vesicular uptake may be a reasonable target for treatment by disease modification.[7]

## Acknowledgment

We acknowledge Janna Gelsomino, RN, for patient care coordination and assistance with research procedures, and Jamie Cherup, CRNP, for conducting research procedures.

## Conflicts of Interest

None of the authors has a commercial relationship with a company whose product is used in the study or may be affected by its outcome.

### References

1. Kaufmann H, Norcliffe-Kaufmann L, Palma JA, et al. Natural history of pure autonomic failure: A United States prospective cohort. Ann Neurol 2017;81(2):287–297.
2. Goldstein DS, Sharabi Y. The heart of PD: Lewy body diseases as neurocardiologic disorders. Brain Res 2019;1 (1702):74–84.
3. Orimo S, Oka T, Miura H, et al. Sympathetic cardiac denervation in Parkinson's disease and pure autonomic failure but not in multiple system atrophy. J Neurol Neurosurg Psychiatry 2002;73:776–777.
4. Goldstein DS, Holmes C, Kopin IJ, Sharabi Y. Intraneuronal vesicular uptake of catecholamines is decreased in patients with Lewy body diseases. J Clin Invest 2011;121 (8):3320–3330.
5. Guo L, Esler MD, Sari C, et al. Does sympathetic dysfunction occur before denervation in pure autonomic failure? Clin Sci 2018;132(1):1–16.
6. Goldstein DS, Pekker MJ, Eisenhofer G, Sharabi Y. Computational modeling reveals multiple abnormalities of myocardial noradrenergic function in Lewy body diseases. JCI Insight 2019;5.
7. Lohr KM, Bernstein AI, Stout KA, et al. Increased vesicular monoamine transporter enhances dopamine release and opposes Parkinson disease-related neurodegeneration in vivo. Proc Natl Acad Sci USA 2014;111(27):9977–9982.
8. Ding YS, Lin KS, Logan J. PET imaging of norepinephrine transporters. Curr Pharm Des 2006;12(30):3831–3845.
9. Schinke C, Hesse S, Rullmann M, et al. Central noradrenaline transporter availability is linked with HPA axis responsiveness and copeptin in human obesity and non-obese controls. Stress 2019;22(1):93–102.
10. Knudsen K, Fedorova TD, Hansen AK, et al. In-vivo staging of pathology in REM sleep behaviour disorder: a multimodality imaging case-control study. Lancet Neurol 2018;17(7):618–628.

 

11. Ding YS, Lin KS, Garza V, et al. Evaluation of a new norepinephrine transporter PET ligand in baboons, both in brain and peripheral organs. Synapse 2003;50(4):345–352.
12. Goldstein DS, Holmes C, Sullivan P, et al. Deficient vesicular storage: a common theme in catecholaminergic neurodegeneration. Parkinsonism Relat Disord 2015;21 (9):1013–1022.
13. Estorch M, Camprecios M, Flotats A, et al. Sympathetic reinnervation of cardiac allografts evaluated by 123I-MIBG imaging. J Nucl Med 1999;40(6):911–916.
14. Kaufmann H. Consensus statement on the definition of orthostatic hypotension, pure autonomic failure and multiple system atrophy. Clin Auton Res 1996;6:125–126.
15. Goldstein DS, Holmes C, Lopez GJ, et al. Cardiac sympathetic denervation predicts PD in at-risk individuals. Parkinsonism Relat Disord 2018;52:90–93.
16. Isonaka R, Rosenberg AZ, Sullivan P, et al. Alpha-Synuclein deposition within sympathetic noradrenergic neurons is associated with myocardial noradrenergic deficiency in neurogenic orthostatic hypotension. Hypertension 2019;73(4):910–918.
17. Goldstein DS, Holmes C, Cannon RO 3rd, et al. Sympathetic cardioneuropathy in dysautonomias. N Engl J Med 1997;336(10):696–702.
18. Bravo PE, Lautamaki R, Carter D, et al. Mechanistic insights into sympathetic neuronal regeneration: Multitracer molecular imaging of catecholamine handling after cardiac transplantation. Circ Cardiovasc Imaging 2015;8(8):e003507.
19. van Ingelghem E, van Zandijcke M, Lammens M. Pure autonomic failure: a new case with clinical, biochemical, and necropsy data. J Neurol Neurosurg Psychiatry 1994;57 (6):745–747.
20. Hague K, Lento P, Morgello S, et al. The distribution of Lewy bodies in pure autonomic failure: autopsy findings and review of the literature. Acta Neuropathol 1997;94 (2):192–196.
21. Arai K, Kato N, Kashiwado K, Hattori T. Pure autonomic failure in association with human alpha-synucleinopathy. Neurosci Lett 2000;296:171–173.
22. Isonaka R, Sullivan P, Jinsmaa Y, et al. Spectrum of abnormalities of sympathetic tyrosine hydroxylase and alpha-synuclein in chronic autonomic failure. Clin Auton Res 2018;28(2):223–230.
23. Isonaka R, Gibbons CH, Wang N, et al. Association of innervation-adjusted alpha-synuclein in arrector pili muscles with cardiac noradrenergic deficiency in autonomic synucleinopathies. Clin Auton Res 2019;29 (6):587–593.
24. Isonaka R, Holmes C, Cook GA Jr, et al. Is pure autonomic failure a distinct nosologic entity? Clin Auton Res 2017;27(2):121–122.
25. Goldstein DS, Sewell L. Olfactory dysfunction in pure autonomic failure: implications for the pathogenesis of Lewy body diseases. Parkinsonism Relat Disord 2009;15 (7):516–520.
26. Kontos HA, Richardson DW, Norvell JE. Norepinephrine depletion in idiopathic orthostatic hypotension. Ann Intern Med 1975;82(3):336–341.
27. Bannister R, Ardill L, Fentem P. Defective autonomic control of blood vessels in idiopathic orthostatic hypotension. Brain 1967;90:725–746.
28. Donadio V, Cortelli P, Elam M, et al. Autonomic innervation in multiple system atrophy and pure autonomic failure. J Neurol Neurosurg Psychiatry 2010;81 (12):1327–1335.
29. Donadio V, Incensi A, Cortelli P, et al. Skin sympathetic fiber alpha-synuclein deposits: a potential biomarker for pure autonomic failure. Neurology 2013;80(8):725–732.
30. Goldstein DS, Eisenhofer G, Dunn BB, et al. Positron emission tomographic imaging of cardiac sympathetic innervation using 6-[18F]fluorodopamine: initial findings in humans. J Am Coll Cardiol 1993;22(7):1961–1971.
31. Goldstein DS, Grossman E, Tamrat M, et al. Positron emission imaging of cardiac sympathetic innervation and function using 18F-6-fluorodopamine: effects of chemical sympathectomy by 6-hydroxydopamine. J Hypertens 1991;9:417–423.
32. Goldstein DS, Chang PC, Eisenhofer G, et al. Positron emission tomographic imaging of cardiac sympathetic innervation and function. Circulation 1990;81:1606–1621.
33. Matsui H, Udaka F, Oda M, et al. Metaiodobenzylguanidine (MIBG) uptake in Parkinson's disease also decreases at thyroid. Ann Nucl Med 2005;19 (3):225–229.
34. Shindo K, Kaneko E, Watanabe H, et al. Analysis of the relationship between muscle sympathetic nerve activity and cardiac 123I-metaiodobenzylguanidine uptake in patients with Parkinson's disease. Mov Disord 2005;20 (11):1419–1424.
35. Kashihara K, Ohno M, Kawada S, Okumura Y. Reduced cardiac uptake and enhanced washout of 123I-MIBG in pure autonomic failure occurs conjointly with Parkinson's disease and dementia with Lewy bodies. J Nucl Med 2006;47(7):1099–1101.
36. Okamura N, Villemagne VL, Drago J, et al. In vivo measurement of vesicular monoamine transporter type 2 density in Parkinson disease with (18)F-AV-133. J Nucl Med 2010;51(2):223–228.
37. Sossi V, de la Fuente-Fernandez R, Schulzer M, et al. Dopamine transporter relation to dopamine turnover in Parkinson's disease: a positron emission tomography study. Ann Neurol 2007;62(5):468–474.
38. Fu JF, Klyuzhin I, McKenzie J, et al. Joint pattern analysis applied to PET DAT and VMAT2 imaging reveals new insights into Parkinson's disease induced presynaptic alterations. Neuroimage Clin 2019;23:101856.


 

39. Lin KJ, Weng YH, Wey SP, et al. Whole-body biodistribution and radiation dosimetry of 18F-FP-(+)-DTBZ (18F-AV-133): a novel vesicular monoamine transporter 2 imaging agent. J Nucl Med 2010;51(9):1480–1485.

40. Goldstein DS, Holmes C, Lopez GJ, et al. Cerebrospinal fluid biomarkers of central dopamine deficiency predict Parkinson's disease. Parkinsonism Relat Disord 2018;50:108–112.

 